



HAL
open science

Intradermal vaccination prevents anti-MOG autoimmune encephalomyelitis in macaques

Claire-Maëlle Fovet, Lev Stimmer, Vanessa Contreras, Philippe Horellou,
Audrey Hubert, Nabila Seddiki, Catherine Chapon, Sabine Tricot, Carole
Leroy, Julien Flament, et al.

► **To cite this version:**

Claire-Maëlle Fovet, Lev Stimmer, Vanessa Contreras, Philippe Horellou, Audrey Hubert, et al.. Intradermal vaccination prevents anti-MOG autoimmune encephalomyelitis in macaques. *EBioMedicine*, 2019, 47, pp.492-505. 10.1016/j.ebiom.2019.08.052 . hal-02305565

HAL Id: hal-02305565

<https://hal.sorbonne-universite.fr/hal-02305565>

Submitted on 4 Oct 2019

HAL is a multi-disciplinary open access archive for the deposit and dissemination of scientific research documents, whether they are published or not. The documents may come from teaching and research institutions in France or abroad, or from public or private research centers.

L'archive ouverte pluridisciplinaire **HAL**, est destinée au dépôt et à la diffusion de documents scientifiques de niveau recherche, publiés ou non, émanant des établissements d'enseignement et de recherche français ou étrangers, des laboratoires publics ou privés.



Research paper

Intradermal vaccination prevents anti-MOG autoimmune encephalomyelitis in macaques



Claire-Maëlle Fovet^{a,1}, Lev Stimmer^{a,1}, Vanessa Contreras^b, Philippe Horellou^b, Audrey Hubert^c, Nabila Seddiki^c, Catherine Chapon^b, Sabine Tricot^b, Carole Leroy^b, Julien Flament^a, Julie Massonneau^{a,d}, Nicolas Tchitchek^b, Bert A. 't Hart^{e,f}, Sandra Zurawski^g, Peter Klucar^g, Philippe Hantraye^a, Kumaran Deiva^b, Gerard Zurawski^g, SangKon Oh^h, Roger Le Grand^b, Ché Serguera^{d,i,*}

^a Commissariat à l'Énergie Atomique (CEA), Molecular Imaging Research Center (MIRcen), 92260 Fontenay-aux-Roses, France

^b CEA, INSERM, Université Paris-Sud, U1184, IDMIT Department, Fontenay-aux-Roses 92265, France

^c Vacine Research Institute, INSERM U955 Institut Mondor de Recherche Biomédicale (IMRB), Créteil, France

^d Laboratoire des Biothérapies, INSERM, UMS27, F-92260 Fontenay-aux-Roses, France

^e Department of Immunobiology, Biomedical Primate Research Centre (BPRC), 2280 GH Rijswijk, the Netherlands

^f University of Groningen, Department of Biomedical Sciences of Cells and Systems, University Medical Center, Groningen, the Netherlands

^g Baylor Institute for Immunology Research (BIIR), Dallas, TX 75204, USA

^h Mayo Clinic, Department of Immunology, Scottsdale, AZ 85259, USA

ⁱ Asfalia Biologics, Institut du Cerveau et de la Moelle épinière (ICM), Hôpital Pitié-Salpêtrière, Paris 75013, France

ARTICLE INFO

Article history:

Received 25 March 2019

Received in revised form 21 August 2019

Accepted 23 August 2019

Available online 3 September 2019

Keywords:

EAE

TGF β

Tolerance

Treg

Anti-MOG IgG

Macaque

ABSTRACT

Background: Autoimmune demyelinating diseases (ADD) are a major cause of neurological disability due to autoreactive cellular and humoral immune responses against brain antigens. A cure for chronic ADD could be obtained by appropriate immunomodulation.

Methods: We implemented a preclinical scheme to foster immune tolerance to myelin oligodendrocyte glycoprotein (MOG), in a cynomolgus-macaque model of experimental autoimmune encephalomyelitis (EAE), in which administration of recombinant human MOG (rhMOG) elicits brain inflammation mediated by MOG-autoreactive CD4⁺ lymphocytes and anti-MOG IgG. For immunotherapy, we used a recombinant antibody (Ab) directed against the dendritic cell-asialoglycoprotein receptor (DC-ASGPR) fused either to MOG or a control antigen PSA (prostate-specific antigen).

Findings: rhMOG and the anti-DC-ASGPR-MOG were respectively detected in CD11a⁺ DCs or CD11b⁺ cells in the skin of macaques. Intradermal administration of anti-DC-ASGPR-MOG, but not control anti-DC-ASGPR-PSA, was protective against EAE. The treatment prevented the CD4⁺ T cell activation and proinflammatory cytokine production observed in controls. Moreover, the administration of anti-DC-ASGPR-MOG induced MOG-specific CD4⁺CD25⁺FOXP3⁺CD39⁺ regulatory lymphocytes and favoured an upsurge in systemic TGF β and IL-8 upon rhMOG re-administration *in vivo*.

Interpretation: We show that the delivery of an anti-DC-ASGPR-MOG allows antigen-specific adaptive immune modulation to prevent the breach of immune tolerance to MOG. Our findings pave the way for therapeutic vaccines for long-lasting remission to grave encephalomyelitis with identified autoantigens, such as ADD associated with anti-MOG autoantibodies.

Fund: Work supported by the French ANR (ANR-11-INBS-0008 and ANR-10-EQPX-02-01), NIH (NIH 1 R01 AI 105066), the Baylor Scott and White Healthcare System funding and Roche Research Collaborative grants.

© 2019 The Authors. Published by Elsevier B.V. This is an open access article under the CC BY-NC-ND license (<http://creativecommons.org/licenses/by-nc-nd/4.0/>).

1. Introduction

Autoimmune demyelinating diseases (ADD) are a major cause of non-traumatic neurological diseases in children and adults. Recent findings show that anti-MOG antibodies (MOG-Abs), recognizing MOG in its native form, are present in a large number of children and adults with ADD [1,2]. These conditions are currently called MOG-Abs-

* Corresponding author at: Asfalia Biologics ICM, Hôpital Pitié-Salpêtrière, Paris 75013, France

E-mail address: che.serguera-y-lagache@inserm.fr (C. Serguera).

¹ Equal contributors.

Research in context

Evidence before this study

Myelin oligodendrocyte glycoprotein (MOG) is a rare myelin autoantigen of human autoimmune demyelinating diseases (ADD), which is frequently used for the induction of experimental autoimmune encephalomyelitis (EAE) in animals. The pathogenesis of ADD associated to anti-MOG antibodies (MOG-Abs) or MOG-Abs-associated diseases implies the breach of immune tolerance against MOG and the activation of MOG-specific T and B cells, which induce inflammatory CNS demyelination. Evidence points to a deficiency of regulatory lymphocytes in human ADD, whereas the mitigation of EAE in mice is observed if MOG is targeted to subsets of tolerogenic dendritic cells (DCs). This induces the differentiation of naïve T cells into FOXP3⁺ regulatory T cells (Tregs) through a TGFβ-dependent mechanism. The DC-asialoglycoprotein receptor (ASGPR) is a scavenger receptor expressed in macaque and human monocyte-derived DCs. Anti-DC-ASGPR antibodies fused to prostate-specific antigen (PSA) injected in macaque skin induce the appearance of PSA-specific suppressor lymphocytes expressing IL-10. Nonetheless, the therapeutic effectiveness of anti-DC-ASGPR immunotherapy remains to be established in a high-fidelity animal model of human CNS autoimmunity.

Added value of this study

Here, we report a therapeutic vaccine that effectively blocks encephalomyelitis in macaques committed to develop EAE after sensitisation with rhMOG emulsified in incomplete Freund's adjuvant (IFA). This immunotherapy focuses MOG entry into CD163⁺ dermal cells through intradermal injection with a humanized anti-DC-ASGPR-monoclonal antibody fused to MOG. This is followed by the appearance of circulating MOG-specific Tregs and complete protection from the disease. The treatment prevents the generation of encephalitogenic CD4⁺ T lymphocytes but does not reduce serum anti-MOG IgG titres. Amidst an on-going debate on the physiopathology of demyelination in MOG-Abs-associated diseases, this protocol demonstrates that serum anti-MOG autoantibodies are not sufficient to trigger brain inflammation and demyelination but require encephalitogenic T cells and blood-brain barrier disruption to enter the CNS. Our results also suggest that peripheral tolerance and immune stimulation are modulated by inversely correlated TGFβ1 and TGFβ2 levels, *i.e.*, active EAE is associated with low systemic TGFβ1 and TGFβ2 levels, whereas induced tolerance is characterised by substantially increased levels of TGFβ1 and TGFβ2, strengthening the evidence that these isoforms of TGFβ contribute to the control of T cell responses.

Implications of all the available evidence

This preclinical protocol for testing vaccine proteins, readily usable in patients, was implemented in a macaque model of autoimmune encephalitis that tightly recapitulates human demyelinating disease with anti-MOG autoantibodies. In the absence of rhMOG/IFA sensitisation, the intradermal administration of the anti-DC-ASGPR-MOG vaccine raised MOG-specific Tregs but did not induce anti-MOG IgG, indicating specificity for Treg induction while not being an immune stimulator. Most importantly, both therapeutic and prophylactic immunotherapy with anti-DC-ASGPR-MOG were highly effective in averting an encephalitogenic immune response to rhMOG/IFA. Thus, anti-DC-ASGPR-MOG might be a novel treatment option to ameliorate MOG-Abs-associated diseases.

associated diseases and can manifest as acute demyelinating encephalomyelitis (ADEM), optic neuritis (ON), transverse myelitis (TM), or neuromyelitis optica spectrum disorder (NMOSD), but rarely as multiple sclerosis (MS) [3,4]. Most patients with relapsing MOG-Abs-associated diseases are dependent on immunosuppressive treatments and B cell depletion, but they respond poorly to MS modifying treatments, which puts humoral immune response at the centre of the pathogenic process [1,2,4]. Moreover, MOG-Abs-associated diseases are characterised by a particular cytokine signature in the cerebrospinal fluid (CSF), further pointing at a pathophysiological process involving antibody opsonisation of myelin [6]. Thus, due to the particular severity of these diseases, although they may in some cases benefit from autologous haematopoietic stem cell transplantation [5], an effective treatment is eagerly awaited, and inducing immune tolerisation to MOG could eventually lead to a cure.

We used a model of experimental autoimmune encephalomyelitis (EAE) in cynomolgus macaques, which shares many clinical-pathological and immunological similarities with MOG Ab-associated ADD and is thus exquisitely useful for investigating innovative therapeutic strategies for these diseases. The model is obtained through administration of a recombinant protein of the extracellular domain of human MOG (rhMOG), emulsified in incomplete Freund's adjuvant (IFA) [7]. MOG is a central nervous system (CNS) restricted myelin protein that is highly prevalent as a target of autoimmunity in ADD [8]. It is also a frequently used antigen to induce chronic EAE in rodents and non-human primates (NHPs) [9]. Cynomolgus macaques sensitised with rhMOG/IFA develop EAE symptoms and harbour brain lesions which can be visualised by MRI. Prominent immunological hallmarks are CD4⁺ T cell reactivity and anti-MOG IgG. Histology of human ADD and monkey EAE shows that lesions detected by brain MRI correspond to demyelination associated with immunoglobulin deposits, complement activation, and the infiltration of neutrophils and macrophages, as well as T and B lymphocytes, suggesting a myelin-directed autoimmune response [7,10].

In animals, EAE is induced through a breach of self-tolerance due to boosted activation of myelin auto-reactive naïve or memory CD4⁺ T cells through MHC-II myelin-antigen presentation by antigen-presenting cells (APCs), such as dendritic cells (DCs). This leads to increased differentiation of CD4⁺ T lymphocytes into encephalitogenic Th1 and Th17 T cells, producing IFNγ or IL-17, respectively, both favouring the infiltration of both lymphocytes and inflammatory phagocytes into the brain white matter [9]. The causes of ADD in humans are not known, but the presence of immune effectors associated with myelin in the brain lesions of patients [10], the response of these diseases to immunosuppressors [2], the increased Th1 and Th17 effector-cell responses in the periphery [6,11], and reported deficient Treg function [12] all indicate an autoimmune course for these diseases, similar to that described for EAE. This also suggests that the pathogenicity of auto-reactive T cells could be counterbalanced by restoring proper Treg function. This idea was corroborated in mouse models of EAE, both *via* adoptive transfer of Tregs [13] and through *in vivo* manipulation of DCs for the induction of MOG-specific Tregs [14,15].

DCs are the most potent APCs and induce and direct adaptive responses towards either immunity or tolerance [16,17]. Hence, DC-targeted vaccines are currently being developed with the clinical purpose of controlling adaptive autoimmune responses [18]. Notably, subsets of immature migratory DCs from the skin, gut, and lungs have tolerogenic properties. In the absence of inflammation, they capture local antigens for presentation to lymphocytes in draining lymph nodes, inducing their differentiation into antigen-specific Treg cells [19]. This is determined by specific co-stimulation of lymphocytes by DCs secreting IL-10 and TGFβ [13,15,20,21].

In human skin, immature dermal DCs, but not Langerhans cells, express the DC-asialoglycoprotein receptor (DC-ASGPR/CLEC10A), a C-type lectin scavenging receptor (CLR) that allows rapid endocytosis of ligands for antigen processing [22]. We previously demonstrated that

antigens (Ags) delivered to skin DCs *via* DC-ASGPR in macaques induce Ag-specific IL-10-producing CD4⁺ T cells with implicit regulatory functions, reminiscent of the T regulatory type 1 (TR1) phenotype [23]. In contrast, targeting of the same Ag to the lectin-like oxidised-LDL receptor (LOX-1) in skin DCs with anti-LOX-1 antibodies induced IFN γ -producing T cell responses [20].

Here we tested the clinical and biological effect of anti-DC-ASGPR-MOG immunotherapy on the occurrence of EAE in a preclinical macaque model of MOG-induced autoimmune encephalomyelitis. We report that the anti-DC-ASGPR-MOG immunotherapy suppresses MOG-induced CNS autoimmunity.

2. Materials and methods

2.1. Animals

We performed our experiments on animals of either sex, as we (unpublished results) and others [7] have shown that sex has no impact on the incidence of EAE. A therapeutic protocol of antigen-specific tolerisation of 90 days was designed using six adult cynomolgus macaques (*Macaca fascicularis*), of which four were female and two were male. We successively implemented a preventive protocol of 120 days using two adult male cynomolgus macaques. All animals came from the MIRCen colony, imported from a licensed primate breeding centre on Mauritius (Cynologics Ltd., Port Louis, Mauritius). For the therapeutic protocol, animals were distributed into two experimental groups of one male and two females each, with no other criteria of selection (Supplemental table 1). The project was run in an agreed user establishment (agreement number 92–032–02) following European Directive 2010/63/UE and French regulations, with institutional permission obtained from the French Ministry of Agriculture after evaluation by an ethical committee (2015081710528804v1). All procedures were performed in compliance with the animal welfare structure of the CEA. Monkeys remained under veterinary care during the study. Before sample collection, immunisation, or treatment, animals were sedated with ketamine hydrochloride (Imalgene, 15 mg/kg, intramuscular injection) and xylazine (2% Rompun, 0.5 mg/kg, intramuscular injection). Anaesthesia was maintained during MRI acquisition with propofol (Propovet, 10 mg/kg/h, intravenous infusion in the external saphenous vein). Individual animal data are listed in Supplemental table 1.

2.2. Study design and power analysis of test group size

In previous experiments, we observed that the incidence of EAE in adult cynomolgus macaques of either sex is 95.45%, as 21 of 22 animals developed the disease following rhMOG/IFA administration, with a mean onset of 34.55 ± 16 days post-immunisation (dpi) or a median of 32 days (our unpublished results). This indicates that each animal has a theoretical probability of 0.9545 to develop EAE under our protocol. We calculated the smallest possible sample of macaques, for ethical reasons and to respect the principle of three Rs (replacement, reduction, and refinement), to prove the concept of therapeutic effectiveness of a molecule for which biological significance had been previously measured using 12 macaques [20]. We used the Fisher Exact test to calculate the smallest possible sample to have no animal developing the disease. We performed this preclinical study on two groups of three animals, either treated with anti-DC-ASGPR-MOG or anti-DC-ASGPR-PSA, as an acceptable level of confidence of 99% leads to an $n = 3$. Only two animals were used in a successive experiment to determine whether intradermal injection of anti-DC-ASGPR-MOG induces anti-MOG IgG. These animals were also used to assess whether pre-treatment with anti-DC-ASGPR-MOG prevents rhMOG/IFA-induced EAE.

2.3. Immunisation and treatment

Animals were administered 300 μ g rhMOG (1 mg/ml) in IFA (Sigma Aldrich) in the dorsal skin by six intradermal injections of 100 μ l (50 μ g rhMOG per injection site) every four weeks until disease onset, as previously described [7]. Six animals received subcutaneous injections of 250 μ g anti-DC-ASGPR-MOG (treated group) or anti-DC-ASGPR-PSA (control group) every week for three weeks, starting from the first week after initial sensitisation with rhMOG/IFA and then one week after each boost with rhMOG/IFA; the doses of anti-DC-ASGPR-MOG or -PSA antibodies were the same as those previously reported [20]. Each animal received a subcutaneous dose of protein in the back between the shoulder blades as five injections of 100 μ l of fusion protein (50 μ g protein per injection site). In a preventive scheme, two macaques received three administrations of anti-DC-ASGPR-MOG every week for three weeks. They were then administered rhMOG/IFA on the fourth week and then again four and eight weeks later. All animals were followed for 90 days after the first rhMOG administration. The scheme of an initial administration of three injections of anti-DC-ASGPR-MOG or anti-DC-ASGPR-PSA, one week apart, was empirically designed to maximise the induction of effector T lymphocytes for both the therapeutic and prophylactic protocols. In the therapeutic protocol, the re-administration of anti-DC-ASGPR-MOG or anti-DC-ASGPR-PSA one week after each boost with rhMOG/IFA was empirically determined to maintain regulatory effector T cell levels.

2.4. Skin DC phenotype

The phenotype of the skin myeloid cells engulfing the injected rhMOG, anti-DC-ASGPR-MOG, or an anti-human CD40-MOG on the human IgG4 heavy chain, as described above and previously [25], was assessed by conjugating the three proteins to Alexa Fluorochrome AF488 or AF594 using a microscale labelling kit (Life technology). Ten μ g of each protein in 100 μ l PBS was injected intradermally in two sites on the back of adult cynomolgus macaques. Skin biopsies (8 mm punch) were surgically removed 4 and 24 h after injection. Tissues were fixed with 4% PFA in PBS once for 6 h, dehydrated in 30% sucrose PBS at 4 °C, embedded in OCT, and frozen at -42 °C. Cryostat sections of 10 μ m were stained with anti-CD163 (GHI-61, 333,602 Biolegend), anti-CD68 (KP1, 344,716 Dako), or anti-CD1a (5C3, M3571 Dako) overnight at 4 °C. A goat anti-mouse IgG1 conjugated to AF594 was used as a secondary antibody. Isotype-specific antibodies were used as negative controls. Tissues were examined using a confocal SP8 microscope (Leica, Germany).

2.5. Clinical observations

Monkeys were observed on a daily basis throughout the experiments. Clinical scores were assessed using a semi-quantitative functional scale, with the severity of disease implying shorter endpoints for the experiments [7] (Supplemental table 2).

2.6. Fluid collection and immunological analysis

Blood was collected each week from the beginning of the protocol, to collect baseline samples, through to EAE and euthanasia, with a total volume of up to 26 ml per month. Cerebrospinal fluid (CSF) was sampled at EAE onset and euthanasia, with up to 500 μ l per puncture. Full haematology with blood cell counts (CBC) was performed at each bleed using an HMX A/L analyser (Beckman Coulter). Immunological investigations were performed with fresh whole blood or isolated peripheral blood mononuclear cells (PBMCs).

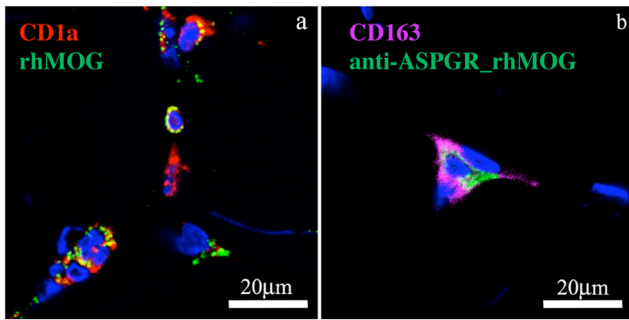


Fig. 1. Skin localisation of the proteins injected into macaques. rhMOG or anti-DC-ASGPR-MOG conjugated to AF488 were injected intradermally and a skin biopsy of the injection site was analysed 4 h later by IHC. a) Detection of rhMOG in CD1a⁺ cells close to the epidermis. b) Co-localisation of anti-DC-ASGPR-MOG with CD163⁺ dermal cells. Nuclei were stained with 4,6 diamidino-2, phenylindole (DAPI) and the tissues analysed by confocal microscopy. Images are representative of ($n > 20$) MOG⁺ cells. See Supplemental fig. 1 for further details.

2.7. T and B cell subsets in the blood

Immunophenotyping was performed on fresh blood at specified time points by flow cytometry using the following antibodies: anti-CD45 (clone D058–1283, Becton–Dickinson (BD) Le Pont-de-Claix, France), anti-CD3 (SP34–2, BD), anti-CD4 (L200, BD), anti-CD8 (BW135/80, Miltenyi Biotec, Paris, France), anti-CD95 (DX2, BD), anti-CD28 (clone 28.2, Beckman Coulter), anti-CD69 (FN50, BD), anti-HLA-DR (clone L243, BD), anti-CD20 (2H7, BD), anti-CD27 (M-T271, Miltenyi), and anti-IgD (rabbit polyclonal, BioRad, Marnes-la-Coquette, France). Briefly, blood was incubated with the mixed antibodies for 15 min, red blood cells were lysed, and the cells were washed and fixed. A total of 10^5 cell events were acquired with a BD LSR II instrument and data was analysed using FlowJo software (Ashland, OR, USA).

2.8. MOG-specific regulatory T cells

Macaque PBMCs (2×10^6 cells/well) were cultured for 44 h (37°C , 5% CO_2) in 500 μl IMDM (ThermoFisher) supplemented with 10% FCS and 1% penicillin/streptomycin, with or without 20 $\mu\text{g}/\text{ml}$ rhMOG. Four hours before the end of incubation, Golgi plug (1 $\mu\text{l}/\text{ml}$, BD Biosciences,) and Golgi stop (0.67 $\mu\text{l}/\text{ml}$, BD Biosciences) were added to the media in each well and the cultures incubated for another 4 h. Cells were washed and stained to detect antigen-specific CD4⁺ T cell subsets, as previously described [26,27], using commercial mAbs according to the manufacturer's guidelines: anti-CD3-BV768 (SP34–2, BD), anti-CD4-BV605 (L200, BD), anti-CD8-APC Cy7 (SK1, Biolegend), anti-OX40-PE (L106, BD), anti-CD25-BV711 (2A3, BD), anti-CD39-PE-CF594 (TU66, BD), and anti-FOXP3-APC (236A/E7, BD). Intracellular staining for FOXP3 required permeabilization buffer and the FOXP3 buffer kit (BD) was used following the manufacturer's instructions. Intracellular staining with anti-IL10-PE (JES3-9D7, BD) and anti-TGF β 1-AF488 (Mouse 9016, R&D system) and extracellular staining with anti-LAP-FITC (TGF β 1) (CH6-17E5.1, Miltenyi Biotec) of macaque PBMCs were also tested but did not permit detection of their targets. Cells were analysed on a three-laser LSR II flow cytometer (BD), with at least 10^5 events collected. FlowJo software was used for analysis.

2.9. Cell-based assay (CBA) for the titration of antibodies to MOG on living cells

HEK293A cells transfected with pIRES2-DsRed2-human MOG (HEK293A_MOG) [28] were used to detect plasma antibody binding to conformationally intact MOG by flow cytometry. Non-transfected HEK293A cells were used as a control. Briefly, 150,000 cells were incubated with plasma at a 1:50 dilution of plasma for 1 h at 4°C . Cells

were then incubated with fluorescein isothiocyanate (FITC) conjugated anti-human IgG + IgA + IgM (H + L) Fab'2 secondary antibody, following the manufacturer's protocol (ref 30446, Kallestad FITC conjugate, Bio-Rad, Marnes la Coquettes, France), or with AF488 goat anti-human IgG1 (1:500, A10631, Invitrogen) for 30 min at 4°C . Cells were fixed in 2% formaldehyde-PBS. A total of 50,000 events per sample were recorded on a FACSCanto II instrument and the data analysed using FlowJo software. Binding was assessed by measuring the mean fluorescence intensity (MFI). Anti-MOG antibody levels are expressed as arbitrary units (AU) of the ΔMFI , determined by the subtraction of the MFI obtained with control HEK293A from that obtained with the HEK293A_MOG cells.

2.10. IgG antibodies

Plasma anti-rhMOG antibody concentrations were assessed by ELISA in 96-well plates. Flat-bottom plastic plates (Costar 3595, Corning) were coated with rhMOG (5 $\mu\text{g}/\text{ml}$ in PBS) overnight at 4°C . After washing and blocking with PBS/1% BSA, the wells were incubated in duplicate with 1:200 or 1:2000 diluted plasma samples. Bound cynomolgus monkey antibodies were detected with alkaline phosphate-labelled goat-anti-human IgG (1:1000, 4H11305, Invitrogen Life Technologies, Bleiswijk, Netherlands) or alkaline phosphate-labelled goat-anti-human IgM (1:2000, A9794, Sigma, St. Quentin Fallavier France). Conjugate binding was quantified with SIGMAFAST *p*-nitrophenyl phosphate (Sigma, St. Quentin Fallavier France). The measured optical density was converted into arbitrary units (AU) using a concentration curve of the same positive control as a reference.

2.11. Cytokine levels in plasma

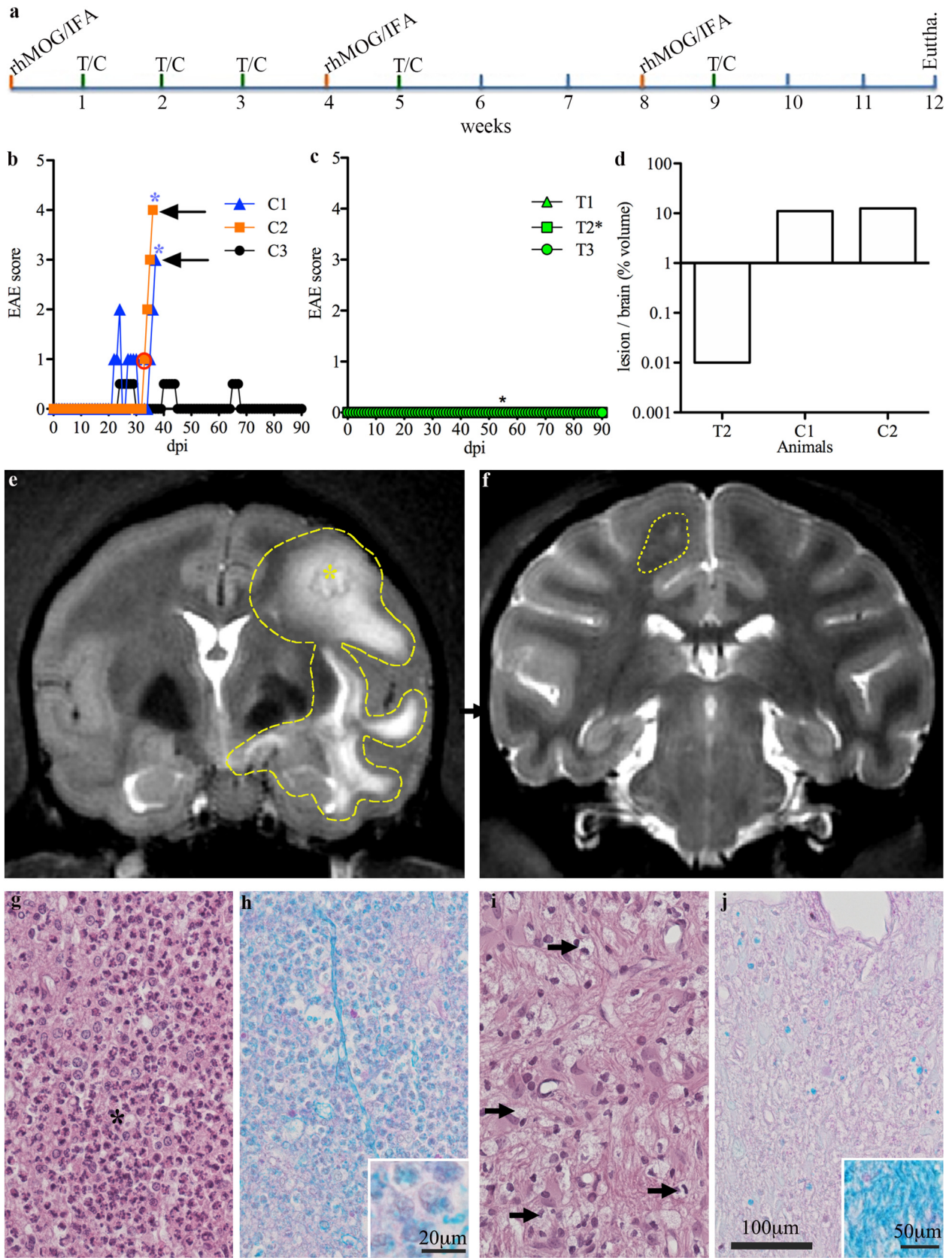
The levels of 15 cytokines were measured in plasma using multiplex technology: MILLIPLEX MAP human Cytokine Magnetic Bead Panel – Customized Premixed 13 Plex (Bulk) Packaging (IL-1 β , GM-CSF, G-CSF, IL-2, IL-4, IL-6, IL-8, IL-10, IL-12p40, IL-17A, TNF α , and IFN γ) and the MILLIPLEX MAP TGF β Magnetic Bead 3 Plex Kit, (TGF β 1, TGF β 2, and TGF β 3), which measures total levels of each of the three isoforms TGF β 1, TGF β 2, and TGF β 3 in serum samples after activation with hydrochloric acid, following the supplier's guidelines (Merckmillipore, Burlington, MA, USA), using a Bioplex 200 (BioRad, Hercules, CA, USA). Quantification of all samples was performed simultaneously.

2.12. MRI acquisition

Magnetic Resonance Imaging (MRI) of anesthetized animals maintained in a stereotaxic frame was performed with a horizontal 7 T Agilent scanner (Palo Alto, CA, USA), using a surface coil for transmission and reception (RAPID Biomedical GmbH, Rimpf, Germany). Lesion segmentation was performed using a high-resolution 2D fast spin-echo sequence. Lesions were delineated manually, slice-by-slice by a single operator, to measure their volume.

2.13. Histology

After euthanasia (Pentobarbital IV, 180 mg/kg), animals were perfused with 2 l of ice cold 4% PFA in PBS. Organs, including the brain, spinal cord, optic nerves, liver, lung, heart, spleen, kidneys, and mesenteric and mediastinal ganglia, as well as injection and immunisation sites, were examined and fixed in 4% PFA for 72 h. All tissues were processed to paraffin blocks, cut, and stained with haematoxylin eosin stain (HE). Brain and spinal-cord sections were stained with luxol-fast-blue (LFB) special stain to assess demyelination. Brain and spinal cord lesions were scored according to their overall severity, number, size, and intralésional myelin loss. For each animal, the whole brain was cut into successive coronal slices of 6 mm. At least one standard tissue section, including both hemispheres from each slice, was stained with HE



and analysed. For the spinal cord, one 6 mm slice was taken from the middle of each segment (cervical, thoracic, lumbar, and caudal) and at least one standard tissue section was stained with HE and analysed. All lesions detected by MRI were collected and serially sectioned for exhaustive analysis by histology and immunohistochemistry.

2.14. Immunohistology

Tissues were dewaxed in xylene and rehydrated. Endogenous peroxidase was suppressed by 0.5% H₂O₂ in methanol. Sections were incubated with rabbit anti-human-IgG (1:100, Sigma, SAB3701291, IgG) and

rabbit anti-human IgM (1:250, Dako). Incubation with primary antibodies was followed by incubation with a biotinylated goat-anti-rabbit antibody for 30 min, followed by incubation with an avidin-biotin-peroxidase complex (Vectastain Elite ABC Kit, Vector Laboratories, PK 6100; Burlingame, CA, USA) for 30 min at room temperature. Positive antigen-antibody reactions were visualised by incubation with 3,3'-diaminobenzidine-tetrahydrochloride (DAB)-H₂O₂ in 0.1 M imidazole, pH 7.1 for 5 min, followed by light counterstaining with HE.

2.15. Statistical analysis

Statistical analyses and graphical representations were performed using Prism 5 (GraphPad Software, Inc). Student's *t*-test (unpaired, two-sided) was used to compare two groups of values. A two-sided one-way ANOVA test with Tukey's multiple comparison was used to compare three groups of values or more. Heatmaps were generated using R software (R Foundation for Statistical Computing, Vienna, Austria) [29]. Hierarchical clustering represented by dendrograms were generated based on the Euclidian distance using the complete-linkage method [30].

3. Results

3.1. Clinical outcome of treatment with anti-DC-ASGPR-MOG

It was previously shown that anti-DC-ASGPR binds to human monocytes and human immature CD14⁺CD1a⁻ monocyte-derived DCs, as well as CD11c⁺ and CD14⁺ cells from macaque PBMCs [22]. In macaque and human skin, it was previously shown that anti-DC-ASGPR binds to CD14⁺CD1c⁺ dermal DCs [20,22,31]. Here, we performed IHC on skin biopsies after intradermal injection of the recombinant proteins to assess whether anti-DC-ASGPR-MOG and rhMOG proteins target the same cells when injected in macaque dermis. We observed localisation of rhMOG and anti-DC-ASGPR-MOG in mutually exclusive dermal cells. The rhMOG entered CD1a⁺ cutaneous DCs, whereas the anti-DC-ASGPR-MOG was found in CD163⁺ dermal cells, likely corresponding to resident macrophages and a subset of monocyte-derived dermal DCs (Fig. 1a and b) [31–33]. Moreover, rhMOG, but not anti-DC-ASGPR-MOG, was associated with the expression of CD40 (Supplemental fig. 1). This shows that anti-DC-ASGPR-MOG binds to resident CD163⁺CD40⁻ dermal cells in an anti-DC-ASGPR mAb-specific manner, whereas rhMOG is phagocytosed by CD1a⁺CD40⁺ Langerhans cells or activated dermal DCs with pro-inflammatory properties [34]. Thus, rhMOG and anti-DC-ASGPR-MOG are phagocytosed by different skin APCs when injected in the dermis.

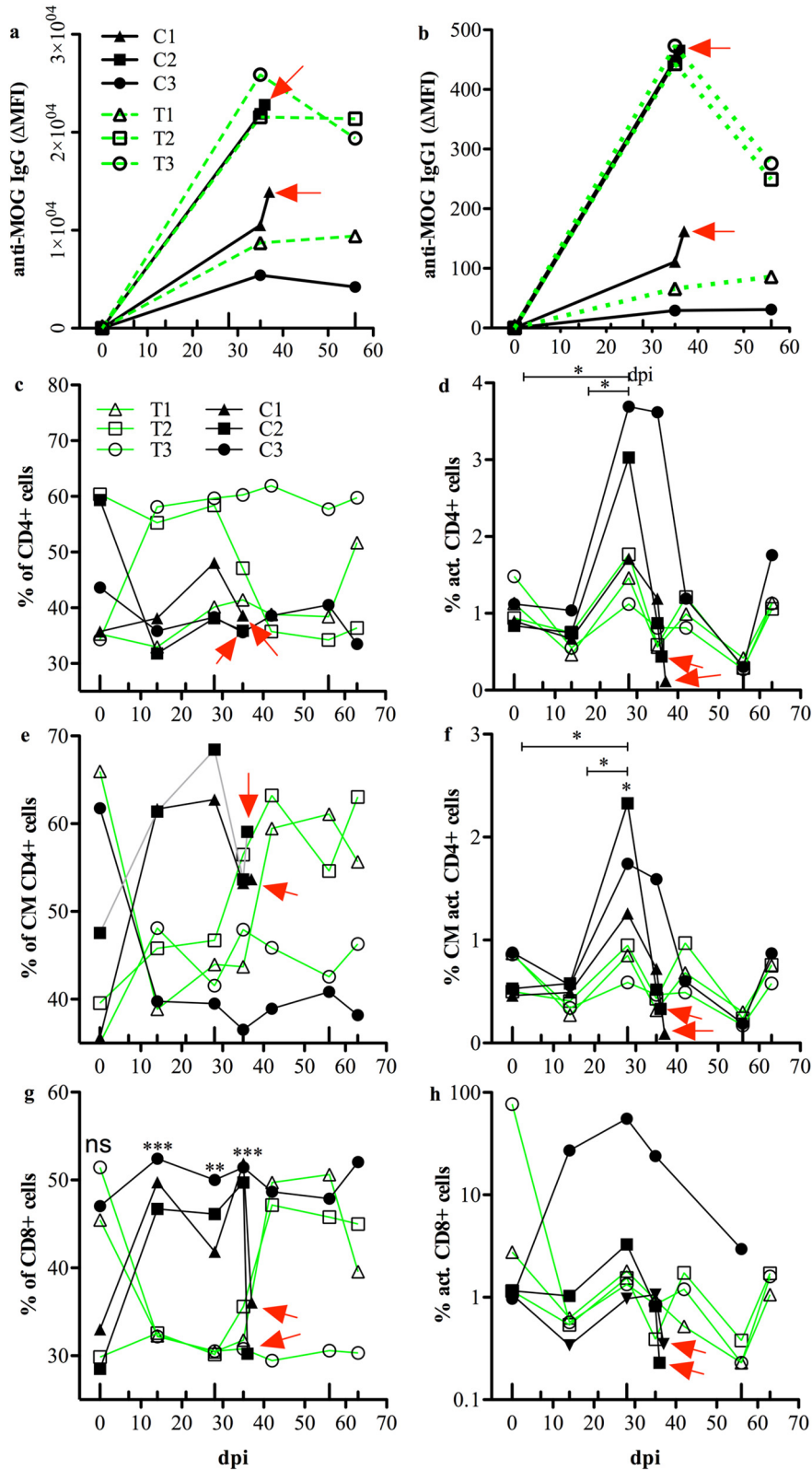
We next assessed whether treatment with the anti-DC-ASGPR-MOG antibody can affect the course of EAE in monkeys. In cynomolgus macaques, rhMOG/IFA administration leads to clinically evident EAE in approximately 35 days [7]. We treated rhMOG-sensitised monkeys

(*n* = 6) with anti-DC-ASGPR-MOG (*n* = 3, animals T1–3) or anti-DC-ASGPR-PSA (*n* = 3, animals C1–3) as detailed in materials and methods and in Fig. 2a. Animals were then examined daily to detect clinical signs of EAE, which were quantified (Supplemental table 2). The three animals receiving the control anti-DC-ASGPR-PSA fusion protein fell ill. Two (C1 and C2) developed classical EAE with the onset at 22 and 32 dpi, evolving towards severe disease after 14 and 3 days, respectively. The third animal (C3) suffered several episodes of paraesthesia and tremor with a low clinical score between 24 and 30 dpi (Fig. 2b). In contrast, none of the three macaques treated with anti-DC-ASGPR-MOG developed clinical signs of EAE within 90 dpi (Fig. 2c). This divergent response to rhMOG immunisation highlights the therapeutic effect of treatment with anti-DC-ASGPR-MOG.

MRI of the two control animals developing severe EAE showed large hyperintense signals at the onset of disease, indicating brain inflammation (Fig. 2e). In contrast, just one animal treated with anti-DC-ASGPR-MOG (T2) showed a lesion during routine MRI at 54 dpi (Fig. 2c and f), but it was approximately 1000 times smaller than those in control animals (Fig. 2d) and was not associated with clinical signs of EAE (Fig. 2b). This lesion was transient, as it was not detected at later MRI timepoints (82 dpi). The other two animals in the treated group developed no detectable lesions. Thus, MRI follow-up showed much greater susceptibility of control animals to develop grave inflammatory brain lesions.

Brain tissues and lesions were analysed by histology at the experimental endpoint after euthanasia at 37 and 36 dpi for animals C1 and C2 or at 90 dpi for the other four animals. Analysis of the brain lesions revealed that the two control animals that developed severe EAE (C1 and C2) showed large lesions of destroyed white matter and some adjacent grey matter. The lesions were round, confluent, and often centred on vascular structures surrounded by necrotic white matter with haemorrhaging and infiltrated by high numbers of degenerated neutrophils and vacuolated macrophages (Fig. 2g). The LFB special stain for myelin revealed demyelination, involving virtually the entire lesion (Fig. 2h). Furthermore, the vacuolated macrophages contained a high amount of phagocytosed LFB-positive myelin debris, as previously observed in acute lesions in this model [7], confirming active demyelination (inset Fig. 2h). Histology of animal T2 confirmed the presence of a small subcortical lesion overlapping the hyperintense signal previously detected by MRI. This lesion contained few vacuolated macrophages and no neutrophils, suggesting healing of an inactive lesion (Fig. 2i). The LFB special stain showed moderate demyelination relative to the surrounding white matter but most macrophages present in the lesion did not contain LFB-positive myelin debris, indicating a chronic inactive lesion (Fig. 2j). HE staining of the brain and spine of the two other anti-DC-ASGPR-MOG treated animals revealed no lesions. Moreover, control animal C3 developed mild EAE, with signs evoking a spinal-cord lesion. However, we were unable to locate its precise position, as our MRI setting did not allow surveying the spinal cord. Macroscopic examination of the spinal cord of this animal at necropsy did not

Fig. 2. Experimental setup, clinical features, imaging, and histology of EAE in treated and control animals. a) A confirmatory preclinical protocol, prospectively powered for clinical outcomes (see study design in material and methods), was carried out over 12 weeks. Six cynomolgus macaques were sensitised with rhMOG/IFA every four weeks (orange ticks), until the onset of EAE. Two groups of three macaques received treatment (green ticks) with anti-DC-ASGPR-MOG (T) or anti-DC-ASGPR-PSA (C) every week for three weeks after the initial immunisation and then every week after the boost with rhMOG/IFA. The onset of EAE was detected through clinical observation of the animals. Behavioural and neurological deficits were measured according to a grid that rates EAE severity (Supplemental table 2). b) Onset and progression of EAE in control animals (C1, C2, and C3) treated with anti-DC-ASGPR-PSA; higher scores reflect more severe illness. Blue stars (*) represent disease-associated brain lesions detected by MRI. c) Onset and progression of disease in animals treated with anti-DC-ASGPR-MOG. Green lines represent the basal scores of treated animals (T1, T2 and T3) and the black star represents an asymptomatic brain lesion detected by MRI. d) Volume of brain lesions detected by MRI in a control and two treated animals. e) Large hyperintense lesion imaged in animal C2 at 35 dpi, encircled by the dotted line. f) Small cortical lesion detected at 54 dpi in animal T2, encircled by the dotted line. From g–j): Brain histopathology of white matter lesions in control (g and h) and treated (i and j) animals, magnification 400×; (g and i) Haematoxylin Eosin (HE) staining; (h and j) Luxol-Fast-Blue-PAS (LFB) stain for myelin fibres. (g) Lesion of a control animal, showing severe myelin degeneration with the infiltration of numerous neutrophils (dark polymorphic nuclei) and a low number of activated microglia/macrophages (to the right of the black star). i) The lesion detected in one treated animal is infiltrated only by a few activated microglia/macrophages (black arrows). h) Severe ongoing myelin phagocytosis in a lesion of a control animal, as revealed by numerous LFB-positive granules in inflammatory cells (inset: magnification of the image, showing phagocytic cells with cytoplasmic vacuoles containing myelin). j) Demyelinated lesion in the treated animal with poor LFB staining and few LFB-positive granules in macrophages; (inset: normal LFB staining at the periphery of the lesion). During the course of this study, we performed many MRI acquisitions but most were normal. EAE in the control animals was severe, with a rapid evolution. The consecutive MRIs in one case (C1) were not informative concerning the progression of the lesions, which remained equally widespread for approximately one week. In the second animal (C2), MRI and the indication of euthanasia were quasi-concomitant, leaving little time to follow the lesions. Only the lesion detected in the one treated animal (T2) could be followed, but it disappeared two weeks after its first detection. Nonetheless, all acquisitions were analysed and processed, especially to assess the volume of the lesions, as reported.



show haemorrhaging and a post-mortem anatomopathological analysis of successive sections of the spinal cord, taken every 2 cm from the cervical to lumbar segments and stained with HE, did not show evidence of immune infiltrate at these locations. We concluded that the animal had had a transient inflammatory episode and dismissed further histological assessments. A more detailed description of the lesions is provided in

Supplemental table 3. Thus, this analysis showed that, relative to the lesion observed in the one treated animal, control animals had wider and more destructive lesions, with substantial disruption of the blood-brain barrier and massive entry of MOG Abs and complement activation, with consequent recruitment of neutrophils and macrophages, leading to tissue destruction. The analysis of the lesion detected in the one treated

animal showed instead a much smaller and self-limiting demyelinating lesion with minor tissue destruction, suggesting containment of the blood brain barrier disruption limiting the subsequent entry of immune mediators of inflammation.

3.2. MOG-specific antibody response

We assessed whether treatment with anti-DC-ASGPR-MOG affected anti-MOG immunoglobulin production, as anti-MOG immunoglobulin is a pathologically relevant feature in non-human primate EAE models and in patients with MOG-Abs-associated diseases [4,35]. We measured anti-MOG IgG + IgA + IgM (Ig) and IgG1 in a cell-based assay (CBA), as only antibodies binding conformational epitopes of native MOG are pathogenic [28]. Binding to cellular MOG by all isotypes of plasma Ig displayed individual trends but they were not statistically different between the treated and control animals. Animal C1, which developed a progressive form of EAE, had intermediate levels of anti-MOG Ig. Animal C2, which developed abrupt EAE had elevated anti-MOG Ig levels and animal C3, with mild EAE, had the lowest titre of anti-MOG Ig. These observations are consistent with the severity of disease, as it correlated with the level of anti-MOG Ig. However, treated animals T1 and T2 also had high levels of anti-MOG Ig at 35 dpi and thereafter, but remained resolutely asymptomatic (Fig. 3a). We measured anti-MOG IgG1 in plasma of treated and control animals by CBA, as anti-MOG IgG1 is a more relevant pathogenic feature and the predominant subclass in anti-MOG related encephalomyelitis [36]. Anti-MOG IgG1 levels were 50 to 100 times lower than those of whole anti-MOG Ig but followed a similar individual slope for each animal as pan Ig, likely reflecting a difference in affinity between anti-Ig and anti-IgG1 secondary antibodies for macaque immunoglobulin (Fig. 3b). Nevertheless, these measures indicate that neither the production of anti-MOG Ig, nor that of IgG1, was altered by the treatment with anti-DC-ASGPR-MOG. This experiment also establishes that high levels of circulating anti-MOG IgG1 are not sufficient to trigger clinical EAE. Thus, the pathogenic factor suppressed by the treatment is not related to anti-MOG IgG1. This highlights a primary pathological role for CD4⁺ T lymphocytes in triggering the disease.

3.3. Phenotype of circulating lymphocytes

We investigated whether the administration of anti-DC-ASGPR-MOG affects the blood count of lymphocyte subtypes by assessing differentiation and activation markers in PBMCs of treated and control animals at various time points after rhMOG/IFA administration. The percentage of CD4⁺ T cells tended to increase in treated animals (Fig. 3c), but only control animals showed an increase in the number of activated CD4⁺CD69⁺ T lymphocytes at 14 ($p = .028$) and 28 dpi ($p = .034$) (Fig. 3d). Moreover, the percentage of activated central memory (CM) CD4⁺CD95⁺CD28⁺CD69⁺ T lymphocytes also increased in controls at 28 dpi relative to baseline ($p = .026$) or that of treated animals at the same timepoint ($p = .040$) (Fig. 3f). There was no difference in the percentage of CD8⁺ T lymphocytes between treated and control animals at baseline ($p = .51$) (Fig. 3g). However, the percentage of CD8⁺ cells was significantly higher in control than treated animals at 14 ($p = .0004$),

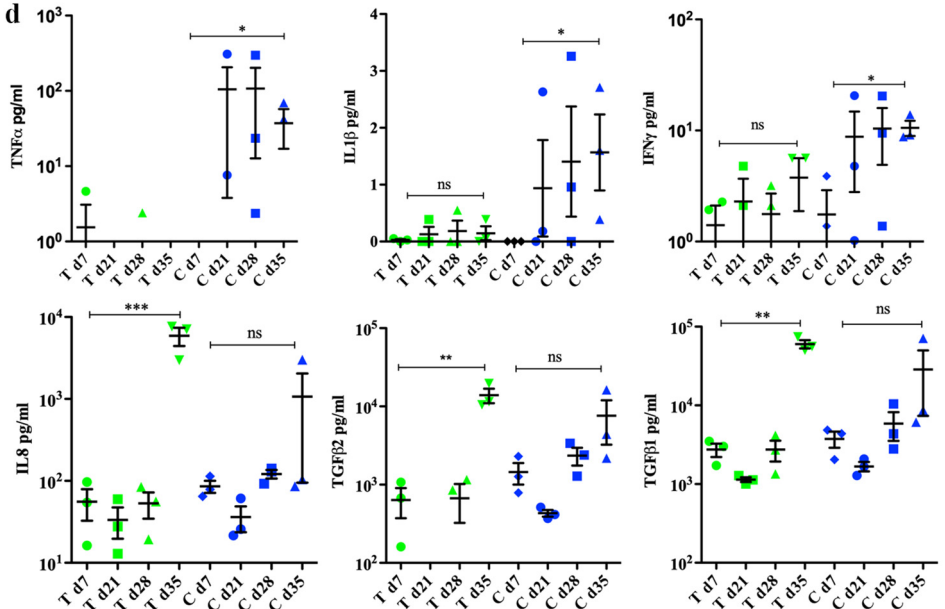
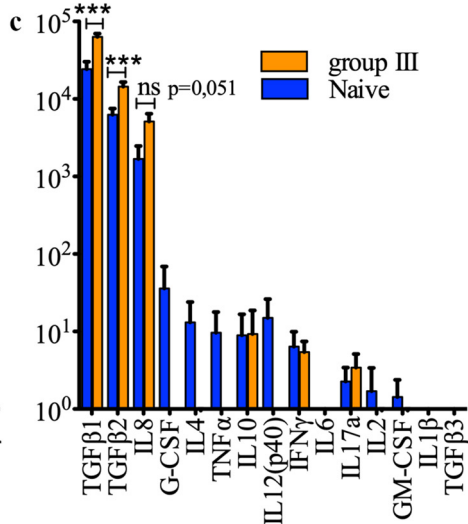
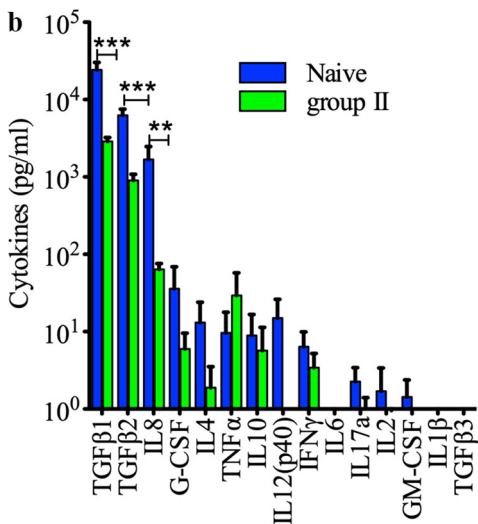
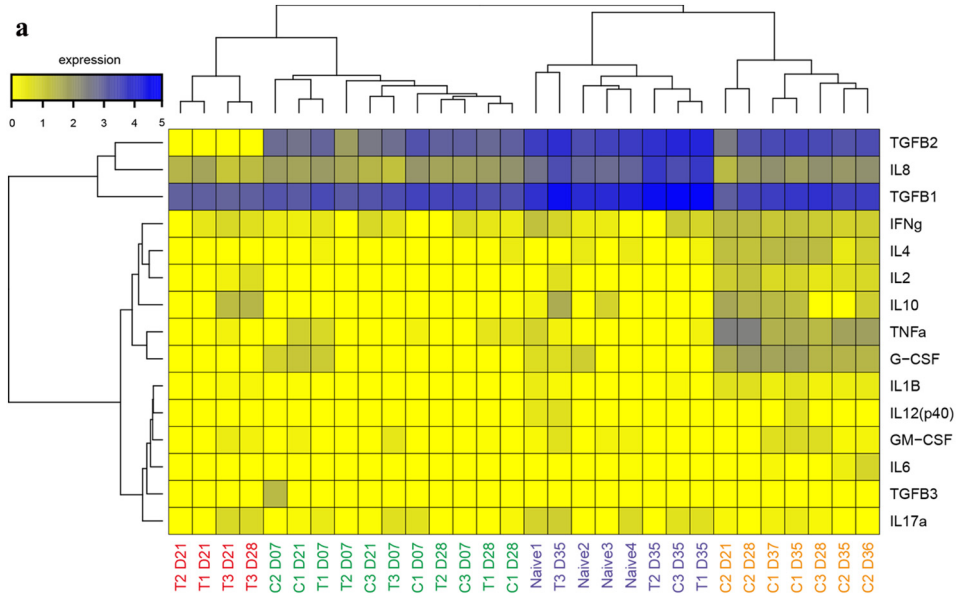
28 ($p = .0027$), and 35 dpi, ($p = .0003$) (Fig. 3g). There was also no difference in the percentage of activated CD8⁺CD69⁺ T cells between treated and control animals (Fig. 3h). Measurement of the absolute number of lymphocytes confirmed the observations based on percentages (Supplemental fig. 3). We assessed other populations of circulating lymphocytes at each timepoint (see examples of gating in Supplemental fig. 4) and observed no differences in the percentage of circulating NK cells or naïve or memory B cells, whether activated or not, between treated and control animals (not shown). Thus, phenotyping of blood lymphocytes showed that the treatment with anti-DC-ASGPR-MOG prevents the activation of naïve and central memory CD4⁺ T lymphocytes and the proliferation of circulating CD8⁺ T lymphocytes in rhMOG/IFA administered animals.

3.4. Cytokine levels in plasma

We measured the levels of 15 cytokines at various timepoints in the plasma of treated and control monkeys and in four naïve animals to further assess any ongoing immune processes associated with anti-DC-ASGPR-MOG treatment. Hierarchical clustering of cytokine levels revealed four groups (Fig. 4a and Supplemental table 4). Group I included only treated animals at 21 and 28 dpi, with particularly low levels of TGFβ2 and high levels of IL-10. Group II was the most heterogeneous and included all treated and control animals at 7 dpi, as well as some animals of either group at 21 or 28 dpi, but no naïve animals, with significantly lower levels of TGFβ1 ($p = .00018$), TGFβ2 ($p = .00002$), and IL-8 ($p = .010$) than naïve animals (Fig. 4b). Group III was comprised of the four naïve macaques, the three treated animals, which were healthy at 35 dpi (one week after the 1st boost with rhMOG/IFA) and control C3 at 35 dpi, in remission from a mild episode of EAE, all displaying high levels of TGFβ1, TGFβ2, and IL-8. Treated macaques in group III showed higher levels of TGFβ1 ($p = .0023$), TGFβ2 ($p = .0066$), and IL-8 ($p = .039$) than naïve animals, which likely reflects basal cytokine levels (Fig. 4c). Group IV included only control animals at the onset or peak of EAE, with lower levels of TGFβ1 ($p = .0083$), TGFβ2 ($p = .015$), and IL-8, ($p = .051$) than naïve animals. A statistical comparison of the cytokine levels in the treated and control groups showed an increase in the level of the pro-inflammatory cytokines TNFα (130×, $p = 0.016$), IL-1β (50×, $p = 0.011$), and IFNγ (6×, $p = .0006$) between 7 and 35 dpi in the three control animals but not the treated animals. Instead, the treated animals showed a 20 to 100-fold increase in the levels of IL-8 (100×, $p = 9E-5$), TGFβ2 (25×, $p = 3E-5$), and TGFβ1 (20×, $p = 3E-7$) from 7 to 35 dpi, whereas the increase in the levels of the same cytokines was only approximately 5- to 10-fold in the controls (Fig. 4d). This confirms the established fact that the onset of EAE is associated with an increase in proinflammatory cytokine levels and suggests that the therapeutic effect of anti-DC-ASGPR-MOG immunotherapy is linked to an increase in TGFβ1 and TGFβ2 levels upon MOG antigen stimulation.

An analysis of individual cytokine levels at various timepoints showed increasing levels of the pro-inflammatory cytokines IFNγ, IL-1β, G-CSF, GM-CSF, and TNFα in the controls, whereas treated animals instead showed a significant increase in TGFβ1, TGFβ2, and IL-8 levels after re-immunisation at 35 dpi. The resilient control

Fig. 3. Levels of anti-MOG IgG and T lymphocyte phenotypes in blood of treated and control animals. a, b) Levels of anti-MOG IgG and IgG1 antibodies in the plasma of treated and control animals, measured by CBA and expressed as the ΔMFI. a) Levels of anti-MOG IgG at baseline and 35 and 56 dpi for all animals, as well as at 36 and 37 dpi for animals C1 and C2, respectively. b) Levels of anti-MOG IgG1. c-h) Phenotype of circulating CD4⁺ and CD8⁺ T lymphocytes assessed by flow cytometry at several timepoints after sensitisation with rhMOG/IFA and expressed as the variation of the phenotype over time, expressed as the percentage (%) of all CD4⁺ or CD8⁺ cells. c) Variations in the percentage of circulating CD4⁺ T cells were not statistically different between control and treated animals. d) Activated CD4⁺CD69⁺ cells increased only in controls at 28 dpi relative to earlier time points. e) The number of central memory (CM) CD4⁺CD95⁺CD28⁺ cells, was not statistically different between the two groups. f) Activated central memory CD4⁺CD95⁺CD28⁺CD69⁺ cells did not significantly increase in control animals at 28 dpi relative to earlier timepoints. g) The percentage of circulating CD8⁺ T cells was statistically higher in control than treated animals after sensitisation with rhMOG/IFA. h) There was no difference in the number of activated CD8⁺CD69⁺ cells between control and treated animals. In all graphs, animals treated with anti-DC-ASGPR-PSA (C1, C2, C3) or anti-DC-ASGPR-MOG (T1, T2, T3) are illustrated with specific symbols (shown in a and c). The large upward ticks on the X axis indicate the administration of rhMOG/IFA; small upward ticks indicate the treatment with anti-DC-ASGPR-MOG or PSA. Red arrows: peak of EAE and euthanasia. Statistics: exploratory analysis using the two-tailed unpaired *t*-test. (*) $p \leq .050$, (**) $p \leq .010$, (***) $p \leq .0010$.



animal, C3, which had developed a mild form of EAE, displayed a peculiar intermediary pattern of cytokines at 28 and 35 dpi, between that seen in animals with full-blown EAE and that seen in treated animals. It combined both patterns of pro- and anti-inflammatory cytokines, suggesting that, at some point, the anti-inflammatory cytokines were sufficient to control disease progression (Fig. 5).

3.5. MOG-specific regulatory cells

TGF β 1, which can be produced by Tregs [37], modulates naïve CD4⁺ T cell physiology, as it can prevent their spontaneous activation, or directly induces their differentiation into FOXP3⁺ Tregs, largely contributing to increasing the threshold of autoimmunity [38–40]. As we measured higher levels of TGF β 1 and TGF β 2 in the plasma of animals treated with anti-DC-ASGPR-MOG after reimmunization with rhMOG/IFA, we assessed whether these animals also showed an increased number of MOG-specific CD3⁺CD4⁺FOXP3⁺ T lymphocytes. We used a sensitive test that measures T cell activation through the detection of the cell surface markers CD25 and CD134 (OX40), which appear after antigen stimulation [41]. Moreover, we measured the expression of the ectoenzyme CD39 to determine whether these cells originated from a subset of resting memory CD39⁺ Tregs, which show suppressive properties and stable expression of FOXP3 [27]. The percentage of MOG-specific CD3⁺CD4⁺CD25⁺OX40⁺ T cells remained at similar levels between control and treated animals at 14 and 35 dpi (Fig. 6a). Among these cells, the frequency of FOXP3⁺CD39⁻ T cells, was not statistically different between treated and control animals at 14 and 35 dpi (Fig. 6b). However, the number of MOG-specific FOXP3⁺CD39⁺ lymphocytes was significantly higher (approximately 2.5-fold) at 35 dpi in treated animals than in the controls ($p = .042$) (Fig. 6c), highlighting an effect of the treatment that favours the development of MOG-specific CD4⁺FOXP3⁺CD39⁺ Tregs.

3.6. Injection with anti-DC-ASGPR-MOG does not raise humoral immunity

We assessed whether the treatment with anti-DC-ASGPR-MOG induces anti-MOG IgG. Two macaques received three injections of anti-DC-ASGPR-MOG at one-week intervals before sensitisation with rhMOG/IFA at the fourth week. We used an ELISA, which is at least 100 times more sensitive than CBA, to detect anti-MOG IgG. Plasma anti-MOG IgG remained at basal levels during treatment with anti-DC-ASGPR-MOG and increased only after rhMOG/IFA sensitisation. This shows that multiple skin injections of anti-DC-ASGPR-MOG does not elicit anti-MOG IgG, even though it carries the exact same protein sequence as rhMOG (Fig. 6d). We also assessed the presence of MOG-specific CD4⁺CD25⁺FOXP3⁺CD39⁺ cells in these two animals. Anti-DC-ASGPR-MOG treatment induced a progressive increase in the number of MOG-specific CD4⁺CD25⁺FOXP3⁺CD39⁺ cells, which reached >50-fold relative to the baseline. Circulating MOG-specific CD4⁺FOXP3⁺CD39⁻ cells were more numerous than CD4⁺CD25⁺FOXP3⁺CD39⁺ cells at earlier time points but tended to decrease during the prophylactic treatment, as they were approximately 2-fold reduced after the third injection with anti-DC-ASGPR-MOG (Fig. 6e). Finally, in

spite of three successive administrations of rhMOG/IFA following the prophylactic treatment, these two animals showed an EAE score of 0 and no brain inflammation by MRI for at least 90 days following the last injection of anti-DC-ASGPR-MOG. Moreover, a systematic post-mortem pathological analysis found no lesions in the brain or spine. These results show that intradermal injection of anti-DC-ASGPR-MOG does not stimulate anti-rhMOG IgG production, whereas it stimulates the appearance of CD4⁺FOXP3⁺CD39⁺ MOG-specific Tregs and prevents EAE in the long-term.

4. Discussion

Autoimmune demyelinating diseases are commonly treated by immunosuppression but more specific immunotherapies, adapted to the physiopathology of each disease and able to restore immune homeostasis, are currently being investigated. Here, we report an effective immune tolerisation scheme that is able to block brain anti-MOG CNS autoimmunity in macaques. Long-lasting disease suppression was based on dermal targeting of the myelin Ag MOG_{1–125} into resident skin DCs and favoured the appearance of MOG-specific Tregs and a dramatic systemic surge of TGF β 1 and TGF β 2 levels upon rhMOG/IFA re-stimulation.

Of the five macaques treated with anti-DC-ASGPR-MOG, none developed EAE over the course of a 90-day experiment, showing that such a tolerogenic strategy, previously shown to mitigate EAE in inbred SPF mice through MOG-targeting to peripheral DCs and the induction of FOXP3⁺ suppressor Tregs [14,15], also applies to outbred adult primates with a rhMOG/IFA-primed immune system. This clinical outcome is remarkable given the very high probability (95%) of any adult cynomolgus macaque to develop severe disease within 35 days after immunisation with rhMOG/IFA (see materials and methods). Indeed, all three control animals treated with anti-DC-ASGPR-PSA developed EAE. This observation establishes that the intradermal routing of MOG into resident DC-ASGPR⁺ cells is sufficient to counteract the breach of tolerance and the induction of MOG-specific autoreactive lymphocytes induced by rhMOG/IFA sensitisation. Phenotyping of blood lymphocytes indicated that only the control animals showed increased activation of CD4⁺ T cells in the days preceding the onset of EAE and a concomitant elevation of proinflammatory cytokines in plasma, which culminated in brain inflammation, demyelination, and EAE, likely amplified by the presence of anti-MOG IgG [42]. In contrast, animals treated with anti-DC-ASGPR-MOG showed an increase in the number of MOG-specific CD4⁺CD25⁺FOXP3⁺CD39⁺ Tregs and a surge in TGF β 1 and TGF β 2 levels upon rhMOG/IFA re-administration, which likely precluded the pathogenic escalation seen in the controls. This recaps a mechanism of TGF β 1-mediated EAE suppression described in mice following oral tolerance [43]. TGF β 1 is a central mediator of peripheral tolerance required to keep naïve T cells quiescent and induce their differentiation into FOXP3⁺ regulatory lymphocytes or FOXP3⁻ suppressor lymphocytes [38,40]. In our experiments, MOG-specific CD4⁺ Tregs induced by the intradermal injection of anti-DC-ASGPR-MOG possibly counteracted the proliferation of MOG-specific autoreactive effectors induced by rhMOG/IFA; this is inferred by the specific absence of activated CD4⁺ T cells and proinflammatory cytokines in the plasma of the treated

Fig. 4. Cytokine levels in plasma of treated and control animals. a) Heatmap showing cytokine levels in the plasma of all animals at several time points after sensitisation with rhMOG/IFA. Cytokine levels are represented by a colour gradient, ranging from yellow (no expression) to deep blue (highest concentration). Hierarchical clustering, represented by dendrograms, was performed at individual and cytokine levels. Four groups of animals were identified and are numbered from 1 to 4 in the text: animals treated with anti-DC-ASGPR-MOG are named T1, T2, and T3, controls treated with anti-DC-ASGPR-PSA, C1, C2, and C3, and untreated non-immunised naïve animals, 1, 2, 3, and 4; timepoints in dpi are numbered from D7 to D37; group I (red), group II (green), group III (purple), group IV (yellow); see also Supplemental table 4). b) Cytokine levels (expressed in log₁₀ of pg/ml) in naïve animals relative to those measured in “EAE incubation” group II, in which there were significantly lower TGF β 1, TGF β 2, and IL-8 levels. c) Cytokine levels measured in “EAE resolution” group III, in which there were significantly higher TGF β 1, TGF β 2 and IL-8 levels in treated animals than naïve macaques. d) Varying cytokine levels between the two groups of treated and control animals and the various timepoints. In green, animals treated with anti-DC-ASGPR-MOG (T); in blue, control animals treated with anti-DC-ASGPR-PSA (C) and timepoints in day (d) post-sensitisation with rhMOG/IFA. The levels of the pro-inflammatory cytokines IL-1 β , IFN γ , and TNF α were elevated at 35 dpi in controls but not treated animals. The levels of IL-8, TGF β 1, and TGF β 2 were elevated in treated animals at the last timepoint of 35 dpi, but not in controls. Statistics: exploratory analysis, with no multiple test correction, using the two-tailed unpaired t-test. (ns) $p > .05$; (*) $p \leq .050$; (**) $p \leq .010$; (***) $p \leq .0010$.

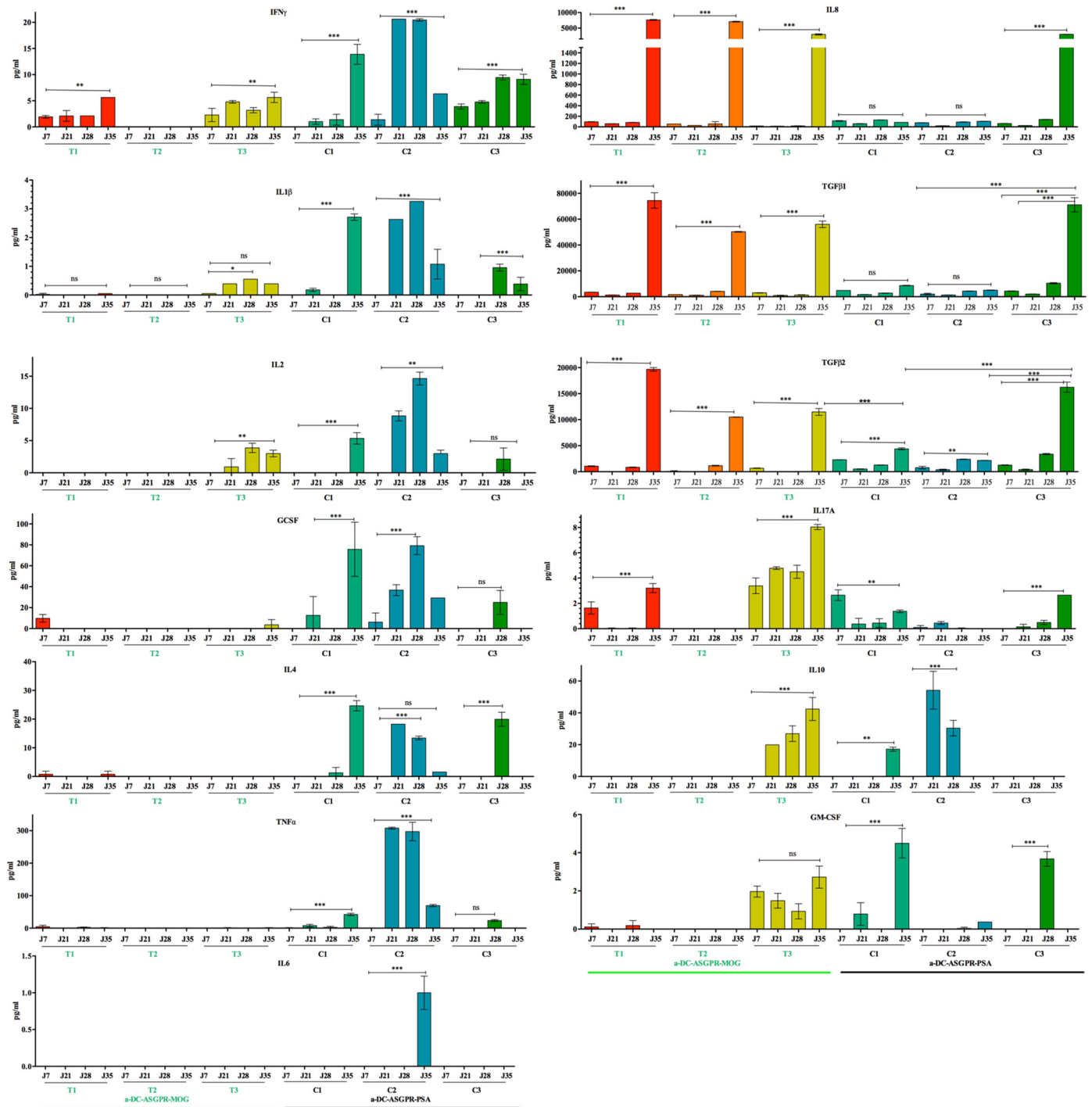


Fig. 5. Cytokine levels per animal at various timepoints. Each bar represents the concentration (pg/ml) of each cytokine in the plasma of animals treated with anti-DC-ASGPR-MOG (T1, T2, T3), underlined in green, and control animals (C1, C2, C3), underlined in black. Bars represent the mean values of two measurements \pm SEM. Statistics: exploratory analysis by one-way ANOVA and Tukey post-test. (ns) $p > .05$; (*) $p \leq .050$; (**) $p \leq .010$; (***) $p \leq .0010$.

animals. Concerning the mechanism of action of the induced MOG-specific Tregs, it is possible that MOG-specific regulatory cells responded to the reinjected rhMOG, upon re-administration of rhMOG/IFA, by increasing the production of IL-8 and TGF β 3, thus attracting neutrophils for antigen clearance while simultaneously preventing adaptive T cell responses to self-antigens, as observed in chronic hepatitis [44]. Alternatively, MOG-specific Tregs may have modulated the skin DC response following the second boost with rhMOG/IFA, favouring the production of TGF β 1 and TGF β 2 by DCs and skewing

naive T cell differentiation towards Tregs and inducing anergy of autoreactive cells [45].

Most interestingly, the monkeys treated with anti-DC-ASGPR-MOG were protected from EAE even though they had elevated levels of circulating anti-MOG IgG. Because an extensive amount of evidence indicates that MOG Abs contribute significantly to inflammation and myelin destruction in EAE models [9,35,42], as well as in patients with MOG Abs-associated diseases [4,6,10], this rather indicates that the brain pathology mediated by MOG Abs requires associated activated

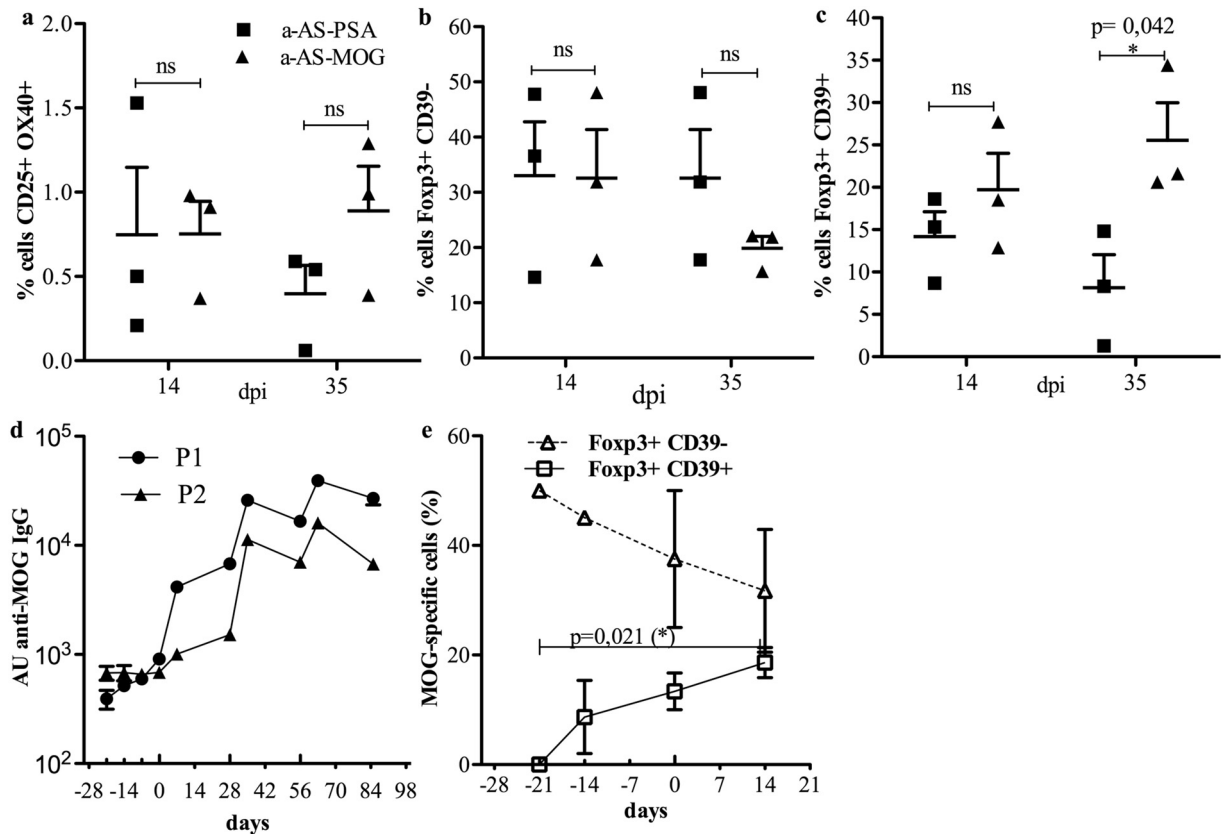


Fig. 6. Measurement of MOG-specific Treg lymphocytes and anti-MOG IgG in treated and control animals. a–c) FOXP3 and CD39 expression among $CD3^+CD4^+CD25^+CD134^+$ T cells during the antigen recall response in macaques sensitised with rhMOG/IFA and receiving anti-DC-ASGPR-MOG or anti-DC-ASGPR-PSA. a) Percentage of $CD3^+CD4^+CD25^+CD134^+$ T cells in PBMCs from treated animals (anti-DC-ASGPR-MOG) or controls (anti-DC-ASGPR-PSA) at 14 and 35 dpi. b) Percentage of $FOXP3^+CD39^-$ cells among $CD3^+CD4^+CD25^+CD134^+$ T cells in treated and control animals. c) Percentage of $FOXP3^+CD39^+$ cells among $CD3^+CD4^+CD25^+CD134^+$ T cells in treated and control animals. d, e) Measurements of anti-MOG IgG and MOG-specific Tregs in two animals injected with anti-DC-ASGPR-MOG prior to sensitisation with rhMOG/IFA. d) Weekly measurement of anti-rhMOG IgG in the plasma of animals by ELISA, expressed as arbitrary units (AU). e) Mean percentage of $CD3^+CD4^+CD25^+CD134^+$ T cells that are $FOXP3^+CD39^-$ (triangles) or $FOXP3^+CD39^+$ (squares) among PBMCs of these two macaques are shown at successive time points. Small upward ticks on the X axis of both graphs indicate anti-DC-ASGPR-MOG injections; large ticks indicate rhMOG/IFA immunisations. Statistics: exploratory analysis, with no multiple test correction, using the two-tailed unpaired t-test. (ns) $p > .050$, (*) $p \leq .050$.

autoreactive T cells. In the course of EAE, these lymphocytes enable the disruption of the brain blood barrier and the entry of pro-inflammatory immune effectors including immunoglobulin [4,42,46], but their presence in macaques treated with anti-DC-ASGPR-MOG is averted by increased numbers of MOG-specific T cells. The fact that macaques with high levels of MOG Abs and elevated amount of MOG-specific Tregs remained healthy, supports the notion that immunotherapy with anti-DC-ASGPR-MOG could effectively prevent relapses in MOG Abs-associated diseases, without depleting B cells, a currently relatively ineffective treatment in these patients [47].

We have previously shown that the fusion of an antigen to anti-DC-ASGPR induces the priming of naïve $CD4^+$ T cells into antigen-specific $IL-10^+$ $FOXP3^-$ suppressors. This same antibody-antigen-fusion vehicle also favoured the appearance of antigen-specific T cells secreting IL-10 when injected into macaque skin, but their precise phenotype was not assessed [20]. Here we show that dermal injection of the anti-DC-ASGPR-MOG antibody induces MOG-specific $CD4^+FOXP3^+CD39^+$ Tregs. It is possible that MOG-specific $IL-10^+FOXP3^-$ suppressors were also induced at specific timepoints of the protocol, but we were not able to detect them due to difficulties in labelling IL-10 in macaque PBMCs. In addition, whether the targeting of DC-ASGPR into cultured IFNDCs or *ex vivo*-derived $CD163^+$ dermal DC/macrophages activates alternative pathways needs to be addressed in future studies. Additional experiments will allow further characterisation of the mechanism of action of such MOG-specific Tregs and better define their pattern of cytokine expression.

Other approaches for the induction of antigen-specific tolerance are currently being explored with varying success. These include the use of nanoparticles for the delivery of peptide antigens, which when coupled to MHC I or MHC II can induce anergy in autoreactive lymphocytes. Other modalities using nanoparticles are under study, including those that target tolerogenic DCs, modulate the inner state of DCs such that they become tolerogenic, or that couple self-antigens to mimic antigen presentation in the context of apoptosis or induction of hepatic or oral tolerance, all of which can induce Treg-dependent tolerance in animal models [48].

Direct manipulations of Tregs has also been envisaged for therapy, either through trophic support of the patients' own Tregs by low-dose administration of IL-2, or T cell therapy through the transfusion of antigen-specific Tregs amplified *ex vivo*, either unmodified or engineered for their expression of a chimeric antigen receptor (CAR) [49,50]. These and other procedures can require complex cell-based manufacturing and provide potential therapeutic benefits that are as yet barely explored in translational medicine. One or more of these approaches may find use in particular diseases, but their medical application will ultimately depend on efficacy and cost.

In conclusion, we report a preclinical protocol based on dermal injection of anti-DC-ASGPR-MOG that induces robust protection of NHP against a grave tissue-specific autoimmune disease. The same approach could be applied to treat autoimmune diseases with any identified autoantigen. As the treatment is effective, in spite of sustained high levels of anti-MOG autoantibodies, patients with autoimmune

demyelinating diseases harbouring anti-MOG or anti-AQP4 IgG could possibly benefit from increasing the pool of MOG- or AQP4-specific Tregs, as anti-MOG or anti-AQP4 autoreactive T cells have been proven to be essential for orchestrating the cascade of pathogenic events characterising these diseases [42].

Funding sources

This work was granted by the French Infrastructures Nationales en Biologie et Santé (INBS) - 2011 Infectious Disease Models and Innovative Therapies (IDMIT), "Programme Investissements d'Avenir" (PIA), Grant number: ANR-11-INBS-0008. The French ANR-10-EQPX-02-01, fund the FlowCyTech facility (IDMIT, Fontenay-aux-Roses, France). The production of the anti-DC-ASGPR-MOG and anti-DC-ASGPR-PSA products was supported by Baylor Scott and White Healthcare System funding, as well as Roche Research Collaborative grants to the Baylor Institute for Immunology Research. SangKon Oh and Gerard Zurawski were also partially supported by the US grant NIH 1 R01 AI 105066. Nicolas Tchitchek was supported by fellowships from the ANRS (France Recherche Nord & Sud Sida-hiv Hépatites).

Author contributions

CS, RLG, and GZ: study design. CS, RLG, KD, and PhHa: supervision of the experiments. AH, CC, CL, CMF, CS, JF, JM, LS, NS, NT, PhHo, ST, and VC: contributed to the acquisition and analysis of the data. CMF, CS, JF, JM, and VC: Animal follow-up, sample collection, and MRI. CMF, CS, JM, and VC: laboratory measurements. AH, CL, NS, and PhHo: cytometry. CC, LS, and ST: tissue treatments and histology. PK, SZ, and GZ provided the key therapeutic reagents used in this study. GZ contributed to the design and optimisation of the anti-DC-ASGPR-antigen fusion proteins used in this study, as well as helping to craft the NHP study design. He also helped draft and edit the manuscript for intellectual content and clarity. PK contributed to the design and optimisation of the anti-DC-ASGPR-antigen fusion proteins used in this study. SZ developed the anti-DC-ASGPR 49C11 hybridoma and supervised production and quality assurance of the anti-DC-ASGPR-antigen fusion proteins used in this study. NS provided key expertise for the detection of MOG-specific Tregs. PhHo provided key expertise to perform the CBA. CMF, CS, LS, NT, and VC: graphs and statistical analysis. B'tH, CMF, CS, GZ, KD, LS, NS, NT, PhH, PK, RLG, SO, and SZ: drafting of the manuscript for main intellectual content. All authors gave final approval to the article.

Declaration of Competing Interest

The authors declare no competing financial interests, except that GZ, SZ, and SKO are inventors on the patent "DENDRITIC CELL ASGPR TARGETING IMMUNOTHERAPEUTICS FOR MULTIPLE SCLEROSIS", held by the Baylor Scott and White Research Institute relevant to the tolerogenic properties of DC-ASGPR targeting (WO2014210540A1), which is directed to anti-DC-ASGPR-MOG/MBP. A granted patent has not yet resulted in this matter at this time. The funders had no role in the study design, data collection, data analysis, interpretation, nor writing of the report.

Acknowledgments

The authors are grateful to Dr. Krista G. Haanstra of the BPRC in Rijswijk, The Netherlands for her help in setting up the EAE model in cynomolgus macaques at MIRCen, CEA, Fontenay-aux-Roses.

Data and material availability

All data associated with this study are available in the main text or the Supplemental materials.

Appendix A. Supplementary data

Supplementary data to this article can be found online at <https://doi.org/10.1016/j.ebiom.2019.08.052>.

References

- [1] Cobo-Calvo A, Ruiz A, Maillart E, Audoin B, Zephir H, Bourre B, et al. Clinical spectrum and prognostic value of CNS MOG autoimmunity in adults: the MOGADOR study. *Neurology* 2018;90:e1858–69. <https://doi.org/10.1212/WNL.0000000000005560>.
- [2] Hacohen Y, Wong YY, Lechner C, Jurynczyk M, Wright S, Konuskan B, et al. Disease course and treatment responses in children with relapsing myelin oligodendrocyte glycoprotein antibody-associated disease. *JAMA Neurol* 2018;75:478–87. <https://doi.org/10.1001/jamaneurol.2017.4601>.
- [3] Jarius S, Ruprecht K, Stellmann JP, Huss A, Ayzenberg I, Willing A, et al. MOG-IgG in primary and secondary chronic progressive multiple sclerosis: a multicenter study of 200 patients and review of the literature. *J Neuroinflamm* 2018;15:88. <https://doi.org/10.1186/s12974-018-1108-6>.
- [4] Reindl M, Waters P. Myelin oligodendrocyte glycoprotein antibodies in neurological disease. *Nat Rev Neurol* 2019;15:89–102. <https://doi.org/10.1038/s41582-018-0112-x>.
- [5] Muraro PA, Martin R, Mancardi GL, Nicholas R, Sormani MP, Saccardi R. Autologous haematopoietic stem cell transplantation for treatment of multiple sclerosis. *Nat Rev Neurol* 2017;13:391–405. <https://doi.org/10.1038/nrneurol.2017.81>.
- [6] Kaneko K, Sato DK, Nakashima I, Ogawa R, Akaishi T, Takai Y, et al. CSF cytokine profile in MOG-IgG+ neurological disease is similar to AQP4-IgG+ NMOSD but distinct from MS: a cross-sectional study and potential therapeutic implications. *J Neurol Neurosurg Psychiatry* 2018;89:927–36. <https://doi.org/10.1136/jnnp-2018-317969>.
- [7] Haanstra KG, Jagessar SA, Bauchet A-L, Doussau M, Fovet C-M, Heijmans N, et al. Induction of experimental autoimmune encephalomyelitis with recombinant human myelin oligodendrocyte glycoprotein in incomplete Freund's adjuvant in three non-human primate species. *J Neuroimmune Pharmacol Off J Soc Neuroimmune Pharmacol* 2013;8:1251–64. <https://doi.org/10.1007/s11481-013-9487-z>.
- [8] Reindl M, Di Pauli F, Rostasy K, Berger T. The spectrum of MOG autoantibody-associated demyelinating diseases. *Nat Rev Neurol* 2013;9:455–61. <https://doi.org/10.1038/nrneurol.2013.118>.
- [9] Hart BA, Gran B, Weissert R. EAE: imperfect but useful models of multiple sclerosis. *Trends Mol Med* 2011;17:119–25. <https://doi.org/10.1016/j.molmed.2010.11.006>.
- [10] Höftberger R, Lassmann H. Chapter 19 - inflammatory demyelinating diseases of the central nervous system. In: Kovacs GG, Alafuzoff I, editors. *Handb Clin Neurol*. Elsevier; 2018. p. 263–83. <https://doi.org/10.1016/B978-0-12-802395-2.00019-5>.
- [11] Sagan SA, Winger RC, Cruz-Herranz A, Nelson PA, Hagberg S, Miller CN, et al. Tolerance checkpoint bypass permits emergence of pathogenic T cells to neuromyelitis optica autoantigen aquaporin-4. *Proc Natl Acad Sci U S A* 2016;113:14781–6. <https://doi.org/10.1073/pnas.1617859114>.
- [12] Brill L, Lavon I, Vaknin-Dembinsky A. Foxp3+ regulatory T cells expression in neuromyelitis optica spectrum disorders. *Mult Scler Relat Disord* 2019;30:114–8. <https://doi.org/10.1016/j.msard.2019.01.047>.
- [13] Selvaraj RK, Geiger TL. Mitigation of experimental allergic encephalomyelitis by TGF-beta induced Foxp3+ regulatory T lymphocytes through the induction of anergy and infectious tolerance. *J Immunol Baltim Md* 2008;180:2830–8.
- [14] Idoyaga J, Fiorese C, Zbytniuk L, Lubkin A, Miller J, Malissen B, et al. Specialized role of migratory dendritic cells in peripheral tolerance induction. *J Clin Invest* 2013;123:844–54. <https://doi.org/10.1172/JCI65260>.
- [15] Ring S, Maas M, Nettelbeck DM, Enk AH, Mahnke K. Targeting of autoantigens to DEC205(+) dendritic cells in vivo suppresses experimental allergic encephalomyelitis in mice. *J Immunol* 2013;191:2938–47. <https://doi.org/10.4049/jimmunol.1202592>.
- [16] Banchereau J, Steinman RM. Dendritic cells and the control of immunity. *Nature* 1998;392:245–52. <https://doi.org/10.1038/32588>.
- [17] Merad M, Sathe P, Helft J, Miller J, Mortha A. The dendritic cell lineage: ontogeny and function of dendritic cells and their subsets in the steady state and the inflamed setting. *Annu Rev Immunol* 2013;31:563–604. <https://doi.org/10.1146/annurev-immunol-020711-074950>.
- [18] Palucka K, Banchereau J, Mellman I. Designing vaccines based on biology of human dendritic cell subsets. *Immunity* 2010;33:464–78. <https://doi.org/10.1016/j.immuni.2010.10.007>.
- [19] Steinman RM, Hawiger D, Nussenzweig MC. Tolerogenic dendritic cells. *Annu Rev Immunol* 2003;21:685–711. <https://doi.org/10.1146/annurev.immunol.21.120601.141040>.
- [20] Li D, Romain G, Flamar A-L, Duluc D, Dullaers M, Li X-H, et al. Targeting self- and foreign antigens to dendritic cells via DC-ASGPR generates IL-10-producing suppressive CD4+ T cells. *J Exp Med* 2012;209:109–21. <https://doi.org/10.1084/jem.20110399>.
- [21] Yamazaki S, Dudziak D, Heidkamp GF, Fiorese C, Bonito AJ, Inaba K, et al. CD8+ CD205+ splenic dendritic cells are specialized to induce Foxp3+ regulatory T cells. *J Immunol Baltim Md* 2008;181:6923–33.
- [22] Valladeau J, Duvert-Frances V, Pin JJ, Kleijmeer MJ, Ait-Yahia S, Ravel O, et al. Immature human dendritic cells express asialoglycoprotein receptor isoforms for efficient receptor-mediated endocytosis. *J Immunol Baltim Md* 2001;167:5767–74.
- [23] Roncarolo MG, Gregori S, Bacchetta R, Battaglia M, Gagliani N. The biology of T regulatory type 1 cells and their therapeutic application in immune-mediated diseases. *Immunity* 2018;49:1004–19. <https://doi.org/10.1016/j.immuni.2018.12.001>.
- [24] Yin W, Gorvel L, Zurawski S, Li D, Ni L, Duluc D, et al. Functional specialty of CD40 and dendritic cell surface lectins for exogenous antigen presentation to CD8(+) T cells.

- and CD4(+) T cells. *EBioMedicine* 2016;5:46–58. <https://doi.org/10.1016/j.ebiom.2016.01.029>.
- [26] Brezar V, Ruffin N, Richert L, Surenaud M, Lacabaratz C, Palucka K, et al. Decreased HIV-specific T-regulatory responses are associated with effective DC-vaccine induced immunity. *PLoS Pathog* 2015;11:e1004752. <https://doi.org/10.1371/journal.ppat.1004752>.
- [27] Seddiki N, Cook L, Hsu DC, Phetsouphanh C, Brown K, Xu Y, et al. Human antigen-specific CD4(+) CD25(+) CD134(+) CD39(+) T cells are enriched for regulatory T cells and comprise a substantial proportion of recall responses. *Eur J Immunol* 2014;44:1644–61. <https://doi.org/10.1002/eji.201344102>.
- [28] Horellou P, Wang M, Keo V, Chretien P, Serguera C, Waters P, et al. Increased interleukin-6 correlates with myelin oligodendrocyte glycoprotein antibodies in pediatric monophasic demyelinating diseases and multiple sclerosis. *J Neuroimmunol* 2015;289:1–7. <https://doi.org/10.1016/j.jneuroim.2015.10.002>.
- [29] R: The R Project for Statistical Computing. <https://www.r-project.org/>; 2019. (accessed August 4, 2019, n.d.).
- [30] Carlsson G, Mémoli F. Characterization, stability and convergence of hierarchical clustering methods. *J Mach Learn Res* 2010;11:1425–70.
- [31] Adam L, Rosenbaum P, Cosma A, Le Grand R, Martinon F. Identification of skin immune cells in non-human primates. *J Immunol Methods* 2015;426:42–9. <https://doi.org/10.1016/j.jim.2015.07.010>.
- [32] Collin M, Bigley V. Human dendritic cell subsets: an update. *Immunology* 2018;154:3–20. <https://doi.org/10.1111/imm.12888>.
- [33] Zaba LC, Fuentes-Duculan J, Steinman RM, Krueger JG, Lowes MA. Normal human dermis contains distinct populations of CD11c+BDCA-1+ dendritic cells and CD163+FXIIIa+ macrophages. *J Clin Invest* 2007;117:2517–25. <https://doi.org/10.1172/JCI32282>.
- [34] Salabert N, Todorova B, Martinon F, Boisgard R, Zurawski G, Zurawski S, et al. Intradermal injection of an anti-Langerin-HIVGag fusion vaccine targets epidermal Langerhans cells in nonhuman primates and can be tracked in vivo. *Eur J Immunol* 2016;46:689–700. <https://doi.org/10.1002/eji.201545465>.
- [35] Genain CP, Nguyen MH, Letvin NL, Pearl R, Davis RL, Adelman M, et al. Antibody facilitation of multiple sclerosis-like lesions in a nonhuman primate. *J Clin Invest* 1995;96:2966–74. <https://doi.org/10.1172/JCI118368>.
- [36] Mariotto S, Ferrari S, Monaco S, Benedetti MD, Schanda K, Alberti D, et al. Clinical spectrum and IgG subclass analysis of anti-myelin oligodendrocyte glycoprotein antibody-associated syndromes: a multicenter study. *J Neurol* 2017;264:2420–30. <https://doi.org/10.1007/s00415-017-8635-4>.
- [37] Li MO, Wan YY, Flavell RA. T cell-produced transforming growth factor-beta1 controls T cell tolerance and regulates Th1- and Th17-cell differentiation. *Immunity* 2007;26:579–91. <https://doi.org/10.1016/j.immuni.2007.03.014>.
- [38] Chen W, Jin W, Hardegen N, Lei K-J, Li L, Marinos N, et al. Conversion of peripheral CD4+CD25- naive T cells to CD4+CD25+ regulatory T cells by TGF-beta induction of transcription factor Foxp3. *J Exp Med* 2003;198:1875–86. <https://doi.org/10.1084/jem.20030152>.
- [39] Gorelik L, Flavell RA. Abrogation of TGFbeta signaling in T cells leads to spontaneous T cell differentiation and autoimmune disease. *Immunity* 2000;12:171–81.
- [40] Tu E, Chia CPZ, Chen W, Zhang D, Park SA, Jin W, et al. T cell receptor-regulated TGF-beta type I receptor expression determines T cell quiescence and activation. *Immunity* 2018;48:745–759.e6. <https://doi.org/10.1016/j.immuni.2018.03.025>.
- [41] Zaunders JJ, Munier ML, Seddiki N, Pett S, Ip S, Bailey M, et al. High levels of human antigen-specific CD4+ T cells in peripheral blood revealed by stimulated coexpression of CD25 and CD134 (OX40). *J Immunol* 2009;183:2827–36. <https://doi.org/10.4049/jimmunol.0803548>.
- [42] Spadaro M, Winklmeier S, Beltrán E, Macrini C, Höftberger R, Schuh E, et al. Pathogenicity of human antibodies against myelin oligodendrocyte glycoprotein. *Ann Neurol* 2018;84:315–28. <https://doi.org/10.1002/ana.25291>.
- [43] Chen Y, Kuchroo VK, Inobe J, Hafler DA, Weiner HL. Regulatory T cell clones induced by oral tolerance: suppression of autoimmune encephalomyelitis. *Science* 1994;265:1237–40.
- [44] Langhans B, Krämer B, Louis M, Nischalke HD, Hüneburg R, Staratschek-Jox A, et al. Intrahepatic IL-8 producing Foxp3+CD4+ regulatory T cells and fibrogenesis in chronic hepatitis C. *J Hepatol* 2013;59:229–35. <https://doi.org/10.1016/j.jhep.2013.04.011>.
- [45] Mavin E, Nicholson L, Rafez Ahmed S, Gao F, Dickinson A, Wang X. Human regulatory T cells mediate transcriptional modulation of dendritic cell function. *J Immunol* 2017;198:138–46. <https://doi.org/10.4049/jimmunol.1502487>.
- [46] Ben-Nun A, Cohen IR. Vaccination against autoimmune encephalomyelitis (EAE): attenuated autoimmune T lymphocytes confer resistance to induction of active EAE but not to EAE mediated by the intact T lymphocyte line. *Eur J Immunol* 1981;11:949–52. <https://doi.org/10.1002/eji.1830111119>.
- [47] Jarius S, Ruprecht K, Kleiter I, Borisow N, Asgari N, Pitarokoili K, et al. MOG-IgG in NMO and related disorders: a multicenter study of 50 patients. Part 2: epidemiology, clinical presentation, radiological and laboratory features, treatment responses, and long-term outcome. *J Neuroinflammation* 2016;13:280. <https://doi.org/10.1186/s12974-016-0718-0>.
- [48] Kishimoto TK, Maldonado RA. Nanoparticles for the induction of antigen-specific immunological tolerance. *Front Immunol* 2018;9. <https://doi.org/10.3389/fimmu.2018.00230>.
- [49] Rosenzwajg M, Lorenzon R, Cacoub P, Pham HP, Pitoiset F, El Soufi K, et al. Immunological and clinical effects of low-dose interleukin-2 across 11 autoimmune diseases in a single, open clinical trial. *Ann Rheum Dis* 2019;78:209–17. <https://doi.org/10.1136/annrheumdis-2018-214229>.
- [50] Sicard A, Boardman DA, Levings MK. Taking regulatory T cell therapy one step further. *Curr Opin Organ Transplant* 2018;23:509–15. <https://doi.org/10.1097/MOT.0000000000000566>.